Int J Infrared Milli Waves (2007) 28:865–879
DOI 10.1007/s10762-007-9264-2

Absorption and Transmission Power Coefficients for Millimeter Waves in a Weakly Ionised Vegetation Fire

Kgakgamatso Mphale · Mal. Heron

Received: 13 March 2007 / Accepted: 27 June 2007 /
Published online: 25 July 2007

Abstract A vegetation fire plume is a weakly ionised gaseous medium. Electrons in the plume are mainly due to thermal ionisation of incumbent alkali impurities. The medium is highly collisional with free electron - neutral particle been the dominant particle interaction mechanism. Signal strength of an incident millimetre wave (MM-Wave) may be significantly attenuated in the plume depending on the extent of ionisation. A numerical experiment was set to investigate signal power loss of a MM-Wave incident on a simulated weakly ionised fire plume with flame maximum (seat) temperature ranging from 1000–1150 K. The simulated fire plume had alkali impurities (potassium) content of 1.0% per unit volume. MM-Wave frequency range investigated in the experiment is from 30–60 GHz. The simulation has application in the prediction of MM-Wave propagation in a crown forest fire and may also be applied in remote sensing studies of forest fire environments. Simulated attenuation per unit path length for the MM-Wave frequencies ranged from 0.06–24.00 dBm^{-1}. Phase change per unit path length was simulated to range from 2.97–306.17°m^{-1} while transmission power coefficients ranged from maximum of 0.9996 for a fire plume at 1000 K to a minimum value of 0.8265 for a plume at a temperature of 1150 K over a plume depth of 1.20 m. Absorption power coefficient ranged from a minimum value of 0.0004 to maximum value of 0.1585 at a seat temperature of 1150 K over the plume depth.

Keywords Signal attenuation · Forest fire · Weakly ionised gas · Ionisation · Phase change

K. Mphale (✉)
Physics Department, University of Botswana, Private Bag 0022, Gaborone, Botswana
e-mail: Mphalekm@mopipi.ub.bw

M. Heron
Marine Geophysical Laboratory, James Cook Univeristy, Townsville, QLD 4811, Australia
e-mail: mal.heron@jcu.edu.au

1 Introduction

Electrons in a highly collisional atmospheric pressure gaseous medium such as vegetation fire may result in a considerable signal power loss for MM-Waves propagating it. When the weakly ionised fire plume is illuminated with electromagnetic wave energy, electrons are perturbed and accelerated by the electric field of the incident waves. If the interaction between electrons and fire neutrals is an elastic one, the neutrals gain little kinetic energy during collisions mainly because they are relatively massive. Electrons are scattered isotropically such that the average velocity after collision is zero. In this way energy is transferred from the MM-Waves to the fire.

Mediterranean regions of Australia and Spain are subject to recurrent large forest fires of varying intensity during dry seasons, which can be up to 90 MWm^{-1}. The maximum flame temperatures of the very high intensity fires can be up to 1300°C [1] and are ionised to the effect of decreasing the efficiency of communication systems in their close proximity [e.g., 2]. The forest fires often result in the destruction valuable vegetation and sometimes can result in loss of human lives, e.g. in [3]. During suppression of the threat, mobile radio communications are in constant use. There are anecdotal reports of failure to maintain (vhf-uhf) radio communication during forest fire suppression, e.g., in [4]. The effect could be severe at MM-Wave frequencies. MM-Wave propagation test conducted on hydrocarbon flames less than 1 m wide at a temperature of close to 1000 K has shown low attenuation values (<5 dB), e.g., in [5], however the attenuation could be higher for very hot (1300°C) ionised flames such as those of a forest fire.

The experiment is a simulation of propagation characteristics of MM-Waves in a weakly ionised line-fire plume with maximum flame temperatures in the range of 1000 K to 1200 K. A flame plasma slab model is used in the numerical experiment to represent fire produced from combusting vegetation e.g., in [6]. The simulation takes advantage of the measured collision frequencies of fire plumes from literature e.g., in [7] to predict; attenuation, phase change, absorption and transmission power coefficients for the MM-Waves in a line-fire plume.

2 Plume ionisation

2.1 Thermal ionisation

The high temperature environment in the fire plume thermally excites some flame particulates to an unstable state. The excitation is on selective basis determined by medium temperature and ionisation potential of the incumbent particles. On collision with other energised flame particles, the excited particulates (S (g)) may shed their outer electrons to become ions according to the following reaction equation.

$$S(g) \Leftrightarrow S^{+}(g) + e^{-} \tag{1}$$

Fire particulates that may appreciably ionise in the flame are alkali impurities and graphitic carbon (C_n).Alkalis have low excitation energy, e.g., potassium and sodium have excitation energies of 4.34 and 5.12 eV respectively. The elements are present in significant quantities in vegetation, e.g., 3.4% of plant's weight is potassium [8]. Carbon can exit in different polymeric forms in the vegetation fire. Graphitic carbon has a low ionisation potential (4.35 eV) and therefore it is an important contributor to thermal ionisation in vegetation fires.

2.2 Chemi-ionisation

Chemi-ionisation is another mechanism by which flame particulates may be ionised in a vegetation litter fire (e.g., in [9]). In the process, dissociation reactions provide part of the energy required for ionization since there are exothermic and the rest is from the fire. Exited methyl radical CH* is a known contributor to chemi-ionisation in flames [10]. CH radical reacts with oxygen atoms in the flame to produce CHO^+, a primary ion in hydrocarbon flames [11] and electrons according to the following reaction equation:

$$CH^* + O \Leftrightarrow CHO^+ + e^- \tag{2}$$

The thermal and chemi-ionisation processes create a weakly ionised environment in the combustion zone.

3 Propagation of MM-Waves in a fire plume

The propagation of MM-waves in a weakly ionised flame is governed by the wave equation

$$\nabla^2 E = \frac{\omega^2 \widetilde{\varepsilon}_r}{c^2} \frac{\partial^2 E}{\partial t^2} \tag{3}$$

where E, ω and $\widetilde{\varepsilon}$ are electric field strength, cyclic propagation frequency (= $2\pi f_0$), complex dielectric permittivity constant respectively. For a plane polarized electromagnetic wave which traverses a nonhomogenous weakly ionised flame in the positive x-direction, its amplitude can be determined by using WKB approximation as in Santoru *et al*., [11];

$$E(x,t) = E_0 \exp\left\{ i\left(\omega.t - \int_0^x \gamma(x)dx \right) \right\} \tag{4}$$

where

$$\gamma = i[\omega/c]\sqrt{\widetilde{\varepsilon}_r} = \alpha_f + \beta_f \tag{5}$$

is the complex wave number and E_0 is the initial electric field strength respectively. α_f and β_f are attenuation and phase constants for the flame. The attenuation and phase constants are given by Akhtar *et al*., [12]. A vegetation fire plume is highly collisional medium with momentum transfer electron - neutral collision frequency up to 10^{12} s^{-1}. When millimetre waves are caused to propagate in a fire plume, expressions for attenuation and phase constants given in [12] reduce to [7]:

$$\alpha_f \cong \frac{\varphi_{eff}}{2c}\left[\frac{\omega_p^2}{(\omega^2 + \varphi_{eff}^2)}\right] \tag{6}$$

and

$$\beta_f \cong \frac{\omega}{c}\left[1 + \frac{\omega_p^4}{8(\omega^2 + \varphi_{eff}^2)^2}\frac{\varphi_{eff}^2}{\omega^2}\right] \tag{7}$$

where φ_{eff} and $\omega_p = \sqrt{Ne^2/m\varepsilon_0}$ are effective electron - neutral collision and plasma frequencies; where also N, e and m are electron density, charge and its mass respectively. ε_0 is dielectric permittivity of free space. Using the WKB approximation, phase shift and

relative attenuation imposed on MM-Waves when they propagate through the plume are given by the expressions [13];

$$\Delta\varphi = \int_0^d \{\beta_0 - \beta(\mathrm{x})\}\mathrm{dx} \tag{8}$$

and

$$\Delta\mathrm{A} = \int_0^d \{\alpha_0 - \alpha(\mathrm{x})\}\mathrm{dx} \tag{9}$$

where α_0 and β_0 are free space attenuation and phase constants.

4 Simulation of a line-fire

Laboratory-scale surface line-fires have been set to study dynamical behaviour of forest fires such as ROS(Rate Of Spread), mass loss rate of vegetation mass and temporal evolution of line fire flame temperature e.g., in [14, 15]. Models were also developed to predict the thermo-physical flame properties of the vegetation fires [14]. The numerical experiment requires an expression for spatial variation of flame temperature as it is required for the evaluation of flame ionisation density and dielectric permittivity.

4.1 Temperature variation across a line- fire

The spatial variation of temperature in a line-fire plume has a Rayleigh profile, e.g., in Mphale *et al*., [6]. According to Mphale *et al*., plume temperature (T_{fl}) is related to the distance from the seat of the fire (b) by the expression:

$$T_{fl} = T_\infty + K\ \exp\left\{\left(-\left(\frac{b}{z}\right)^2\right)\right\} \tag{10}$$

where K and b are experimental constants. From the Rayleigh profile, z denotes distance from an arbitrary origin of the curve. T_∞ is ambient temperature. The temperature is highest at the center (seat) of the fire and decreases exponentially with towards of the edges of the plume.

4.2 Thermal equilibrium assumption

Under normal circumstances, open vegetation fires have temperature gradients which disable the combustion from attaining a Complete Thermal Equilibrium (CTE) state. The dynamics of an open fire is such that volatile combustible particulates are drawn from the surface of combusting vegetation by convective currents to center of the flame where they are involved in exothermic reactions which produce temperatures up to 1300°C, e.g., in Butler *et al*., [1]. Not much of the ambient air reaches the seat of the fire. This leads to insufficient cooling from the ambient air. Therefore temperatures tend to be hottest at the combustion zone and decrease exponentially towards the periphery of fire plume as it is predicted from equation

(10). The non-equilibrium condition in the fire makes it difficult to theoretically determine its radial variation of its dielectric permittivity. However, as a first approximation, the fire volume can be divided into elementary small volumes (ΔV) whose physical parameters such as particle velocity and temperature can be described by their statistical averages $\overline{T}$, $\widetilde{\varepsilon}_r$ and $\overline{v}$. The spatial variation of temperature, relative dielectric permittivity and electron density for the fire plume at any particular height above the combusting fuel surface along the propagation path can then be approximated by a step function (see Fig. 1).

For the assumption to hold, gas particles within the elementary volumes must be involved in a lot of collisions. With average kinetic temperature assigned to elementary volumes, predictions of excitation, gas velocity and degree of ionization using Maxwell-Boltzmann statistics and Saha-Eggert equations are possible. The physical state of the elementary gas volumes can be assumed to be in partial Local Thermodynamic Equilibrium (p-LTE).

4.3 Effective electron-neutral collision frequency of a fire plume

The average effective electron-neutral collision frequency is a factor of neutral gas density, average temperature of the plume and the velocity of plume electrons. The composition of the plume is also very important as effective collision frequency is calculated from weighted averages of constituent gas number densities (n). Major constituents of a fire plume are nitrogen; which forms a large fraction of the combustion mixture, carbon dioxide, carbon monoxide and water vapour. The average effective collision frequency of the fire plume is determined from the relation [16]:

$$\langle \varphi_{\text{eff}} \rangle = \frac{8}{3\sqrt{\pi}} n \left[\frac{m}{2kT}\right]^{5/2} \int_0^{\infty} u^5 Q(u) \exp\left\{-\frac{mu^2}{2kT}\right\} du \tag{11}$$

where n, Q, u, k, T are neutral gas density, momentum transfer collision cross section for a neutral gas, electron gas velocity, Boltzmann's constant and temperature of the plume respectively. However, Itakawa [16] has composed data for combustion gas collision cross

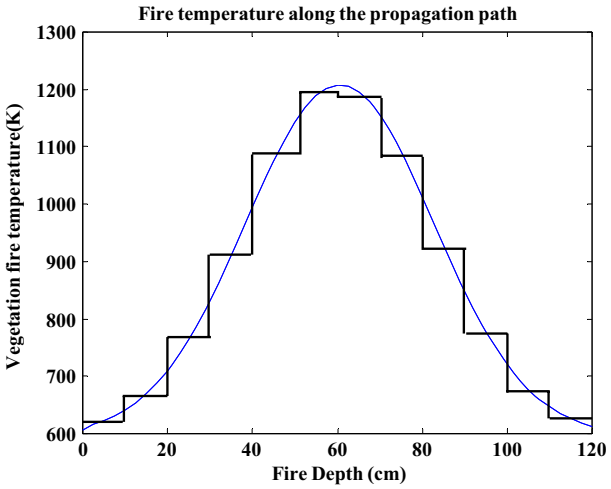

Fig. 1 Step function approximation of temperature at any height above fuel surface.

sections for temperatures up to 3000°C. When the data is used for possible plume composition and temperature, effective collision frequencies in the range of $3 \times 10^{10} - 3 \times 10^{11}\,\mathrm{s}^{-1}$ are obtained.

4.4 Ionization and dielectric permittivity of the fire plume

Potassium compounds and atoms form a large fraction of ionisable particulates in combustion volatiles. The volatiles are released from the vegetation's organic matrix and drawn into the combustion zone of the fire by convective currents. The potassium compounds are first decomposed into respective atoms and the later species are ionized upon excitation. Atoms of potassium result from reduction of potassium-charcoal (K–O–C) complex by hydrogen radical [17]. Basing on Okuno *et al*., [17], the numerical experiment considers volatilised potassium atoms only. The radial temperature and other physical properties of the fire plume such as electron density in the propagation path are averaged over elementary volumes (see Section 4.2). Considering the assumptions, then the mass of potassium drawn into the flame with the volatiles per a unit time (K_{mass}) can be given by the relation;

$$K_{mass} = \frac{V_f.P_k}{V_v}(\mathrm{kg}) \tag{12}$$

where P_k is percentage of potassium in vegetation on dry weight basis while V_f and V_v represent volatile flux and vertical velocity respectively. The number of potassium atoms (μ) swept into a unit volume in a unit time is

$$\mu = \frac{K_{mass}.A_v}{0.03903}(\mathrm{atoms}) \tag{13}$$

where $A_v = 6.02 \times 10^{23}$ (Avogadro number). Electron density (N_e) can be estimated to be [18];

$$N_e = \left(K_I N_p\right)^{1/2}\left[\left(1 + \frac{K_1}{4N_p}\right)^{1/2} - \left(\frac{K_1}{4N_p}\right)^{1/2}\right] \tag{14}$$

where K_I is ionisation equilibrium constant and N_p is the total number of ionised potassium particles given by;

$$N_p = 7.335 \times 10^{27}\mu/T \tag{15}$$

The ionisation equilibrium constant for ionisation (K_I) is given by Saha equation as;

$$K_I = \frac{2P_{m^+\,int}}{P_{mint}}\left(\frac{2\pi.M_e kT}{h^2}\right)^{3/2}\exp\left(\frac{-(E_i)}{kT}\right) \tag{16}$$

where P_{mint} and $P_{m^+\,int}$ are internal partition function of particles; E_i, M_e, k and h are ionization energy, mass of an electron, Boltzmann and Plank constants respectively. Complex dielectric permittivity of a weakly ionised highly collisional gas at millimeter wavelengths is given by the expression:

$$\widetilde{\varepsilon}_r = 1 - i\left\{\frac{\omega_p^2}{\left(\omega^2 + \varphi_{eff}^2\right)}\left(\frac{\varphi_{eff}}{\omega}\right)\right\} \tag{17}$$

where the parameters are as defined in earlier sections. It is a factor of both ionisation and collision frequency and therefore its axial variation in the plume is also a step function.

4.5 Calculation of power absorption and transmission coefficients

For the propagation of MM-Waves at normal incidence to the fire plume, the reflection coefficient equation at (m+1)th elementary volume of the composite in Fig. 2 is given by Laurrossi *et al*., [19] as;

$$R_{m+1} = \frac{E_r}{E_o} = \frac{\left(\frac{\varepsilon_{m+1}}{\varepsilon_m}\right) - \left(\frac{\varepsilon_{m+1}}{\varepsilon_m}\right)^{1/2}}{\left(\frac{\varepsilon_{m+1}}{\varepsilon_m}\right) + \left(\frac{\varepsilon_{m+1}}{\varepsilon_m}\right)^{1/2}} \tag{18}$$

Transmitted power coefficient (P_{tf}) for the whole slab arrangement is given by Tang *et al*., [20] as;

$$P_{tf} = \prod_{1=1}^{sn} \left(\left(1 - |R_{m+1}|^2\right) [\exp\left(-2\alpha_f(i)d\right)] \right) \tag{19}$$

Total reflected power fraction for the composite is also given by Tang *et al*., [20] as;

$$P_{rf} = \left\{ R_1^2 + \sum_{i=2}^{sn} \left[(R_i)^2 \prod_{i=1}^{sn-1} \left(\left(1 - |R_i|^2\right) (\exp\left[-4(i)\alpha_f\, d\right]) \right) \right] \right\} \tag{20}$$

5 Numerical simulation of MM-Wave propagation characteristics in fire

5.1 Simulated flame electron density and dielectric permittivity

The numerical experiment simulates the propagation of MM-Waves through a vegetation fire slab which has spatially varying thermo-physical properties e.g., dielectric permittivity. The fire seat temperature at the fuel surface is assumed to range from 1000–1200 K. Assuming that the fire plume is in p-LTE state, the spatial variation of temperature, ionisation

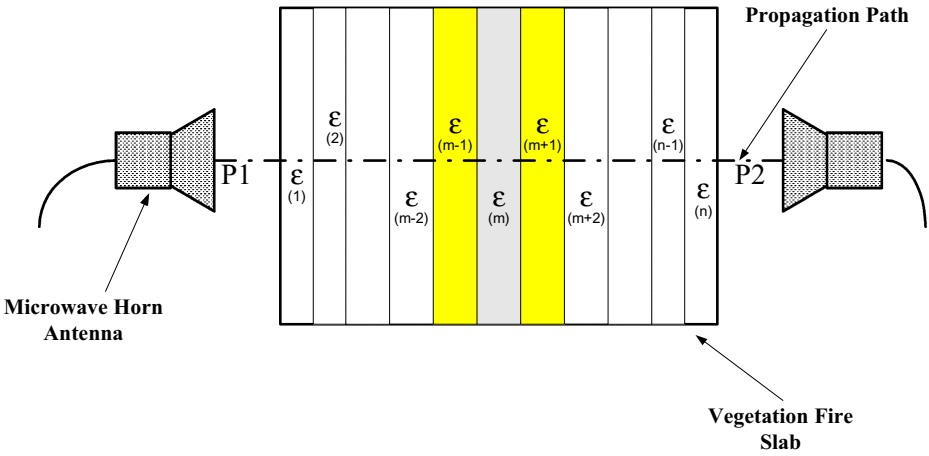

Fig. 2 A possible experimental set up for fire absorptivity and transmissivity.

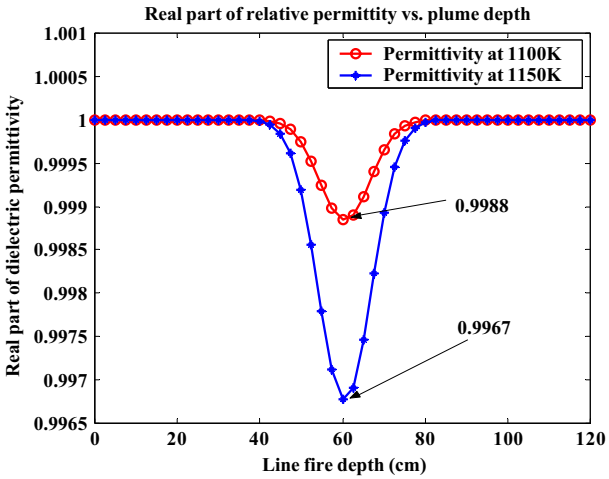

Fig. 3 Variation of real part of dielectric permittivity along the propagation path.

and hence dielectric permittivity at any height above the fuel surface has a Gaussian profile. The wave propagation is through the plume centre such that it is perpendicular to the plume periphery in any direction. The propagation path is P1–P2 as shown in Fig. 2.

At MM frequencies, the complex dielectric permittivity of the plume decreases from the edges of the fire to a minimum value at the seat of the fire. The variation of the dielectric permittivity along the propagation path is step function which has lowest value at the centre. The step width of the function is the width of the elementary volume discussed in Section 4.2. *In the approximation (Fig. 2), $\varepsilon_{(m+1)} < \varepsilon_{(m+2)}$ as this is temperature dependent. Figure 3 *shows spatial variation of dielectric permittivity along the propagation path for a fire plume *with seat temperatures of 1100 and 1150 K. The step function does not show clearly because of a small step width used in the simulation. For temperatures considered, dielectric permittivity can be as low as 0.9967.

*The approximation of spatial variation of electron density along the propagation path at any height above the fuel surface is determined from equation (14). At a temperature of 1100 K, flame electron density is predicted to rise exponentially from a very low value at the edges of the plume to about 1.32×10^{16} m^{-3} at the seat of the fire. For the fire with seat temperature of 1150 K, maximum electron density is predicted to be up to 3.70×10^{16} m^{-3} (see Fig. 4).

6 Numerical results and discussions

6.1 Attenuation and phase change

6.1.1 Attenuation and phase shift for a shrub fire at seat temperature of 1000 K

Attenuation and phase change imposed on MM-Waves by a fire plume was determined from equations (8) and (9). From the simulations, signal attenuation due to a fire plume with maximum seat temperature of 1000 K increased with the increase in momentum transfer collision frequency for the three frequencies considered. When MM-Waves with frequencies 30–60 GHz traversed the plume, attenuation in the range of 0.07–0.84 dB were observed. The attenuation range predicted from the simulation is less than 5 dB and this

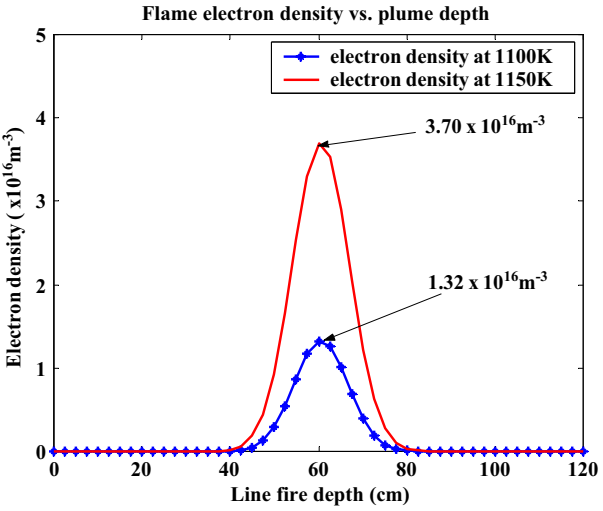

Fig. 4 Variation of electron density across the fire plume along propagation path.

agrees well with propagation tests results in [3]. Generally, Signal attenuation decreased with the increase in MM-Wave frequency over the collision frequency range considered. The attenuation increased smoothly for the frequencies 45 and 60 GHz.This was not so with a 30 GHz signal which was observed to have a peak attenuation of 0.84 dB at a collision frequency of 1.8×10^{11} s^{-1} (see Fig. 5). Phase change decreased with the increase in MM-Wave frequency from 3.56–10.78 degrees from 30–60 GHz at least for collision frequencies less than 2×10^{11} s^{-1} (Fig. 6a, b. After the collision frequency of 2.31×10^{11} s^{-1}, the phase change for the 30 GHz signal fell rapidly to values lower than those of 45 GHz and it continued to fall to phase shifts less than those of 60 GHz after a collision frequency of 2.67×10^{11} s^{-1}.

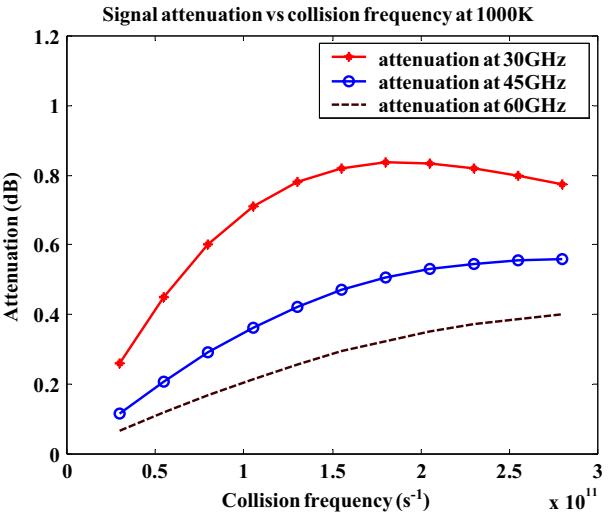

Fig. 5 Signal attenuation vs. collision frequencies at 1000 K.

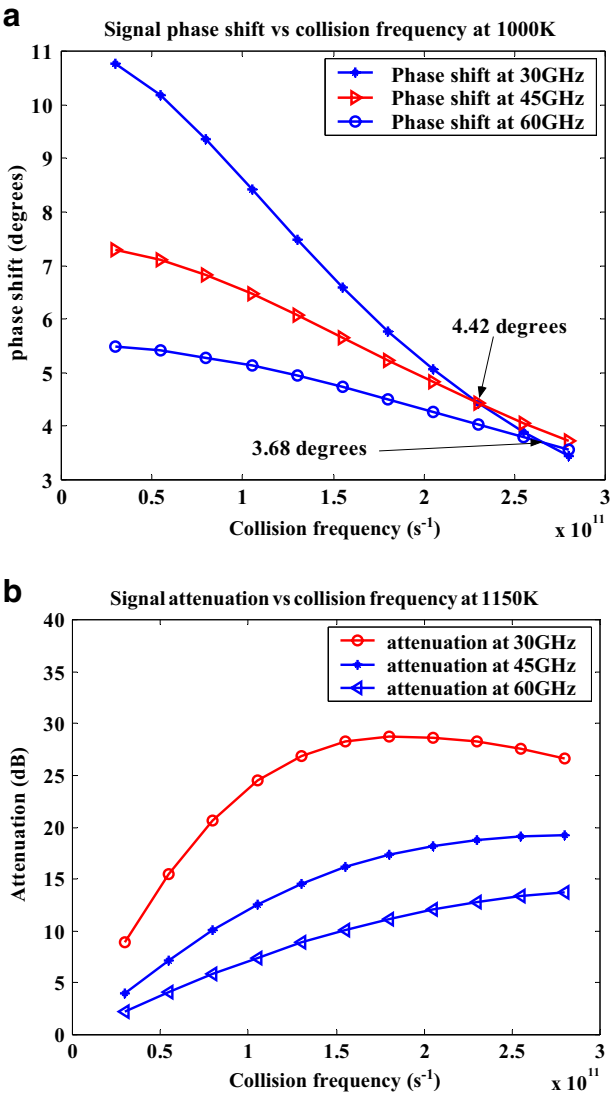

Fig. 6 (**a**) Signal phase change for vs. collision frequencies at 1000 K. (**b**) Signal attenuation vs. collision frequencies at 1150 K.

6.1.2 Attenuation and phase shift for a shrub fire at seat temperature of 1150 K

Signal attenuation imposed by a fire plume at maximum temperature of 1150 K also increased with increase in momentum transfer electron - neutral collision frequency. Comparatively, the attenuations are higher than those due to a fire plume at 1000 K. Attenuation imposed on a 30 GHz signal increased from 8.93 dB at a collision frequency 3×10^{10} s^{-1} to a maximum of 28.80 dB at a collision frequency of 1.8×10^{11} s^{-1}. This corresponds to attenuation per unit path length of 24.00 dBm^{-1}. The attenuation did not continue to rise, however it steadily decreased to 26.66 dB at 2.8×10^{11} s^{-1}. However, signal attenuation peak is not observed with the other two MM-Wave frequencies (see Fig. 6b). The 45 GHz signal attenuation has been observed to increase from 4.00 dB at

3×10^{10} s^{-1} to maximum value of 19.19 dB at 2.8×10^{11} s^{-1}. This corresponds to average attenuation per unit path length of 16.00 dBm^{-1}. The 60 GHz signal attenuation also increased from a minimum of 2.28 dB at 3×10^{10} s^{-1} to a value of 13.77 dB, thus a attenuation per unit path length of 11.50 dBm^{-1}.

Signal phase change varied with the increase in collision frequency for the considered MM-Wave frequencies. The behaviour of signal phase shift imposed by a plume at a maximum temperature of 1150 K is very similar to that imposed by a plume a maximum temperature of 1000 K except in phase change magnitude. Phase shift on the 60 GHz signal steadily decreased from a maximum valve of 188.79degrees to a value of 122.43degrees at a collision frequency of 2.8×10^{11} s^{-1}. Phase shift for the 45 GHz signal also fell from a maximum of 250.53degrees at 3×10^{10} s^{-1} to a value of 127.88degrees at 2.8×10^{11} s^{-1}. The 45 GHz phase change graph fell faster that of 60 GHz (see Fig. 7). The rate of decrease of phase change for the 30 GHz signal was the highest of the two frequencies. It can be observed from Fig. 7 that the graph cuts the other (45 and 60 GHz) graphs. It crosses the 60 GHz graph at the collision frequency of 2.67×10^{11} s^{-1} and that of 45 GHz at 2.3×10^{11} s^{-1}.

6.1.3 Absorption and transmission coefficient at maximum temperature of 1000 K

Millimetre wave transmission power coefficient in a shrub fire of maximum seat temperature of 1000 K has been observed to generally increase with an increase in propagation frequency at least up to the collision frequency of 1.8×10^{11} s^{-1}. At the signal frequency of 30 GHz, transmission coefficient decreased from a maximum of 0.9983 to a minimum of 0.9945 at the collision frequency of 1.8×10^{11} s^{-1}. The transmission power coefficient then rises to a value of 0.9949 at the collision frequency of 2.8×10^{11} s^{-1}. At 45 GHz, the signal transmission power coefficient steadily decreases from a value of 0.9992 to a value of 0.9963. A similar trend is observed for a MM-Wave signal at 60 GHz. Transmission power coefficient decreased from 0.9996 to 0.9974.

Absorption coefficient is also observed to follow a similar trend though in the opposite direction. The 60 GHz signal is the least absorbed. Signal absorption coefficient at the frequency is observed to rise steadily from a low value of 8.82×10^{-4} at a collision frequency

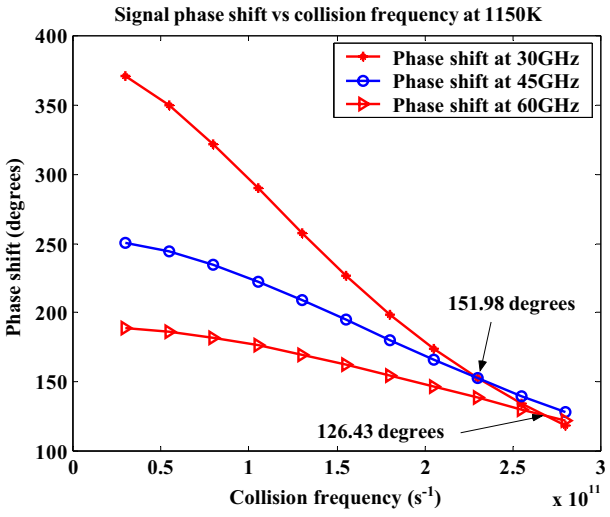

Fig. 7 Signal phase change vs. collision frequencies at 1150 K.

of 3×10^{10} s^{-1} to a value of 5.30×10^{-3} at 2.8×10^{11} s^{-1}. The 45 GHz signal followed a similar behaviour with power absorption coefficient increasing from 1.55×10^{-3} at a collision frequency of 3×10^{10} s^{-1} to a value of 7.37×10^{-3} at 2.8×10^{11} s^{-1}. However, the absorption coefficient for the 30 GHz signal did not rise steadily like the other two signals. It increased from a low value of 3.44×10^{-3} to maximum of 1.10×10^{-2}. It then decreases steadily to a value of 1.02×10^{-2} at 2.8×10^{11} s^{-1}. This corresponds to attenuation per unit path length of 2.40 dBm^{-1}. The attenuation did not continue to rise, however it steadily decreased to 26.66 dB at 2.8×10^{11} s^{-1}. However, signal attenuation peak is not observed with the other two MM-Wave frequencies (see Fig. 6b). The 45 GHz signal attenuation has been observed to increase from 4.00 dB at 3×10^{10} s^{-1} to maximum value of 19.19 dB at 2.8×10^{11} s^{-1} (Fig. 8b).

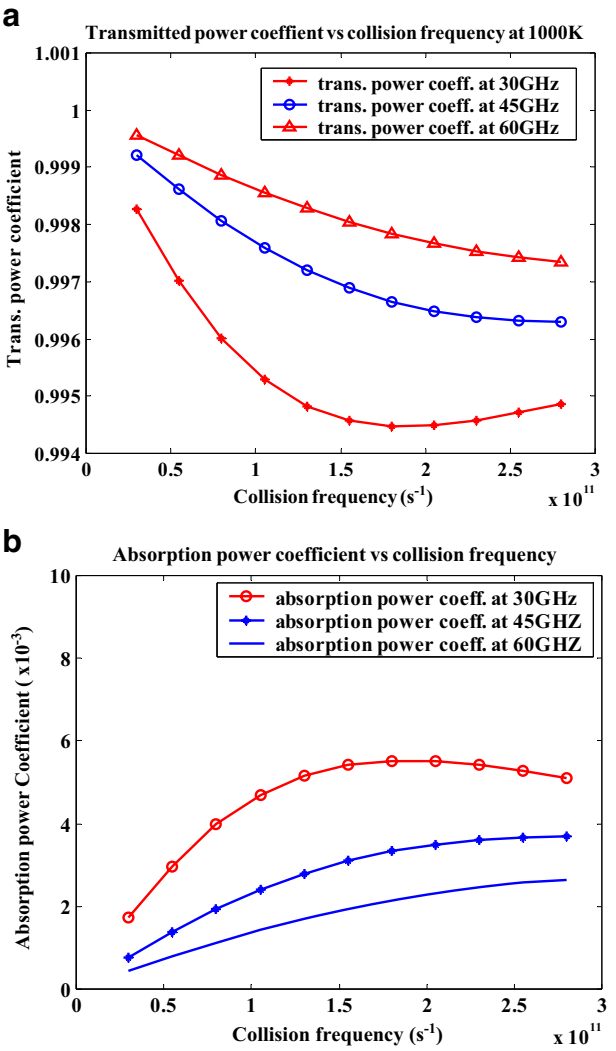

Fig. 8 (**a**) Signal transmission power coeff. vs. collision frequencies at 1000 K. (**b**) Signal absorption power coeff. vs. collision frequencies at 1000 K.

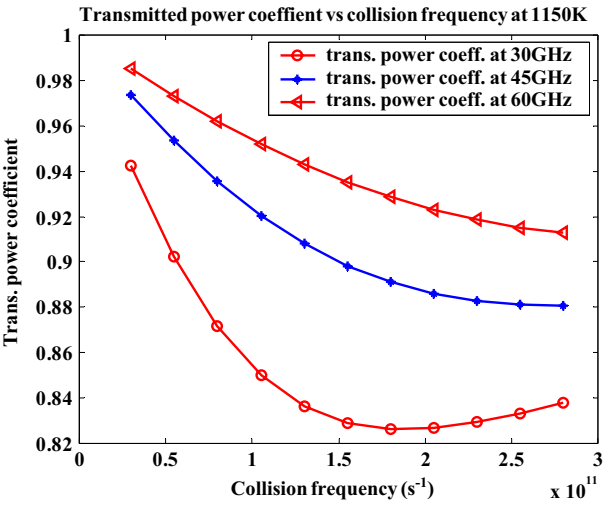

Fig. 9 Signal power transmission coeff. vs. collision frequencies at 1150 K.

6.1.4 Absorption and transmission coefficient at maximum temperature of 1150 K

Shrub fire at the temperature of 1150 K seems to hot enough to cause significant ionisation as there is significant decrease in the transmission coefficient of MM-Waves more especially the 30 GHz signal. Transmission coefficient of the 30 GHz signal was observed to decrease from 0.9425 at the collision frequency of 3×10^{10} s^{-1} to a minimum of 0.8265 at 1.8×10^{11} s^{-1} and steadily rose to 0.8379 at 2.8×10^{11} s^{-1} (Fig. 9). There was a steady decrease in transmission coefficient for the other two MM-Wave frequencies. For the 45 GHz signal, transmission coefficient decreased from 0.9737 at 3×10^{10} s^{-1} to a low value of 0.8806 at 2.8×10^{11} s^{-1} (see Fig. 9). A similar trend was observed for the 60 GHz, transmissivity fell

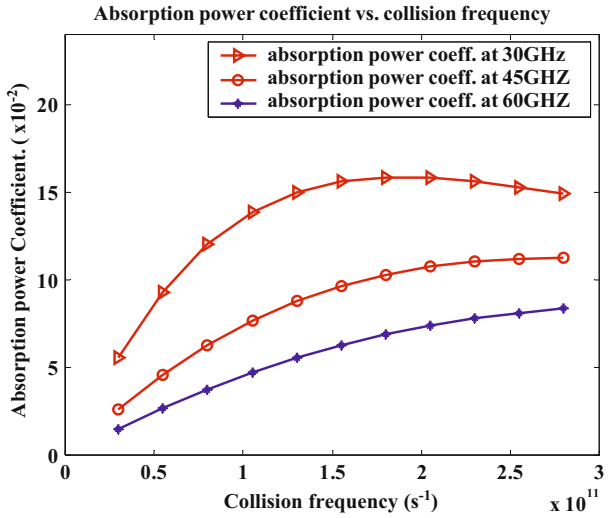

Fig. 10 Signal power absorption coeff. vs. collision frequencies at 1150 K.

from a value of 0.9850 at collision frequency of 3×10^{10} s^{-1} to a value of 0.9127 at 2.8×10^{11} s^{-1}. From the simulation, it appears that the 60 GHz is the least affected by collisional absorption while the 30 GHz signal appears to be most affected.

Absorption coefficient for MM-Wave signals was observed to increase with the increase in plume collision frequency. At any particular collision frequency within the range considered, absorption coefficient decreased with the increase in propagation frequency. At 60 GHz, the power absorption coefficient increased from a minimum value of 2.97×10^{-2} to a value of 16.7×10^{-2} within the frequency range considered. A steady increase from absorption coefficient of 5.20×10^{-2} to 22.47×10^{-2} was observed at the propagation frequency of 45 GHz (Fig. 10). The 30 GHz signal's absorption coefficient was observed to rise steadily from 11.18×10^{-2} to a maximum of 31.70×10^{-2} at the collision frequency of 1.8×10^{11} s^{-1} and the steadily fall to a value of 29.79×10^{-2} at 2.8×10^{11} s^{-1} (see Fig. 10).

7 Conclusions

Attenuation per unit path length for a MM wave signal in a simulated shrub fire with maximum temperature of 1000 K varies from 0.06–0.70 dBm^{-1}. This is increased to range from 7.44–24.00 dBm^{-1} for a shrub fire with maximum temperature of 1150 K and potassium content of 1.0%. Signal attenuation is a factor of both temperature and potassium impurities in flame. It appears that at particular temperature and alkali content in the flame, MM-Wave frequency bands are the most affected. Mphale *et al*., [6] have predicted very high frequency (vhf) signal attenuation per unit path lengths in the range of 0.001–0.49 dBm^{-1} for a grassfire with potassium content of 2.0% and temperature range of 1000 – 1200 K. The attenuation per unit length in a grassfire was also measured to be in the same range. At microwave frequencies, attenuation per unit path length was measured by Mphale *et al*., [7] to be in the range 1.95–11.36 dBm^{-1} for vegetation litter flame with maximum temperature of about 1100 K. However, within the frequency band such as the MM-wave frequencies considered in the numerical simulation, 60 GHz was the least affected as it had the lowest attenuation for a given collision frequency.

The signal phase changes imposed on the MM-Waves by the simulated fire plume with maximum seat temperature of 1000–1500 K ranged from 3.56–371 degrees for the collision frequencies considered in the experiment. The highest phase shift is that imposed on the 30 GHz signal. The phase change could be a factor of alkali content in flame, e.g., Mphale *et al*., [6], who carried out a propagation experiment at vhf with a flame which varied in potassium content. Comparing the results of Mphale *et al*., [6] with those from the experiment and considering that the potassium content in the experiment is 1.0%, it can be observed that the millimetre waves are the most affected. Within the frequency band, the 60 GHz is the least affected with the maximum phase change per unit length of $157.32°m^{-1}$ for a plume with seat temperature of 1150 K.

Absorption power coefficient for the plume with seat temperature of 1000 K ranged from 0.04 to 0.55% in the collision frequency range of $3\times10^{10}-2.8\times10^{11}$ s^{-1} for the MM-Wave frequencies considered. Since there was negligible reflection for millimetre waves from the plume, transmission power coefficient ranged from 0.9996 to 0.9945. For the fire plume at a maximum temperature of 1150 K, absorption power coefficient ranged from a minimum of 0.0149 to a maximum of 0.1585. Transmission power coefficient was observed to vary from a minimum value of 0.8265 to a maximum value of 0.9850.

Acknowledgements We would like gratefully to acknowledge the Staff Development Office of the University of Botswana. The work was partly supported by Emergency Management Australia under project no. 60/2001.

References

1. B. W. Butler, J. Cohen, D. J. Latham, R. D. Schuette, P. Sopko, K. S. Shannan, D. Jimenet, and L. S. Bradshaw, Measurements of radiant emission power and temperature in crown fires. Can. J. For. Res. **34**, 1577–1587 (2003).
2. T. Foster, *Bushfire: History, Prevention and Control* (A. H. and A.W. Reed Pty Ltd, Sydney, 1976).
3. P. R. Williams, R. A. Congdon, and P. Clarke, Effect of fire regimes on plant abundance in tropical eucalyptus savanna of North-Eastern Australia. Aust. Ecol. **28**, 324–338 (2003).
4. D. W. Williams, J. S. Adams, J. J. Batten, G. F. Whitty, and G. T. Richardson, "Operation Euroka: An Australian Mass Fire Experiment," Report 386, Defense Standards Laboratory, Maribyrnor, Victoria Australia, 1970.
5. C. J. Gibbins and R. Chadha, Millimetre-wave propagation through hydrocarbon flame, IEE Proc., H Microw. Antennas Propag. **134**, 169–173 (1987).
6. K. M. Mphale and M. Heron, Plant alkali content and radio wave communication efficiency in high intensity savanna wildfires, J. Atmos. Sol.-Terr. Phys. **69**, 471–484 (2007).
7. K. Mphale, M. Jacob, and M. Heron, Prediction and measurement of electron density and collision frequency in a weakly ionised pine fire, Int. J. Infrared Millim. Waves **28**, 251–262 (2007).
8. M. Radojevic, Chemistry of forest fires and regional haze with emphasis on Southeast Asia, Pure Appl. Geophys. **12**, 157–187 (2003).
9. D. Latham, Space charge generated by wind tunnel fires, Atmos. Res. **51**, 267–278 (1999).
10. C. J. Butler and A. N. Hayhurst, Kinetics of gas-phase ionization of an alkali metal, A, by the electron and proton transfer reactions: A + H_3O^+ → A +.H_20 +H; AOH + AOH2+ H20 in fuel-rich flames at 1800–2250 K, J. Chem. Soc. Faraday Trans. **98**, 2729–2734 (1998).
11. J. Santoru and D. J. Gregorie, Electromagnetic wave absorption in highly collisional plasma, J. Appl. Phys. **74**, 3736–3743 (1993).
12. K. Akhtar, E. J. Scharer, S. M. Tysk, and E. Kho, Plasma interferometry at high pressures, Rev. Sci. Instrum. **74**, 996–1001 (2003).
13. S. Zang, X. Hu, Z. Jiang, M. Liu, and Y. He, Propagation of an electromagnetic wave in an atmospheric pressure plasma: Numerical solutions, Phys. Plasmas **13**, 013502 (2006).
14. J. L. Dupuy and M. Larini, Fire spread through a porous forest fuel bed: A radiative and convective model including fire-induced flow effect, Int. J. Wildland Fire **9**, 155–172 (1999).
15. T. Marcelli, P. A. Santoni, A. Simeoni, E. Leoni, and B. Porterie, Fire spread across pine needle fuel beds: Characterization of temperature and velocity distributions within the plume, Int. J. Wildland Fire **13**, 37–48 (2004).
16. Y. Itikawa, Effective collision frequency of electrons in gases. Phys. Fluids **16**, 831–835 (1973).
17. T. Okuno, N. Sonoyama, J. Hayashi, C. Li, C. Sathe, and T. Chiba, Primary release of alkali and alkaline earth metallic species during pyrolysis of pulverized biomass, Energy Fuels **19**, 2164–2171 (2005).
18. L. S. Frost, Conductivity of seeded atmospheric pressure plasmas, J. Appl. Phys. **32**, 2029–2036 (1961).
19. M. Laroussi and J. R. Roth, Numerical calculation of the reflection, absorption and transmission of microwave by a nonuniform plasma slab, IEEE Trans. Plasma Sci. **21**, 366–372 (1993).
20. D. L. Tang, A. P. Sun, X. M. Qiu, and P. Chu, Interaction of electromagnetic waves with a magnetized nonuniform plasma slab, IEEE Trans. Plasma Sci. **31**, 405–410 (2003).